

The Diabatic Contour Advective Semi-Lagrangian Model

DAVID G. DRITSCHEL

School of Mathematics and Statistics, University of St Andrews, St Andrews, United Kingdom

MAARTEN H. P. AMBAUM

Department of Meteorology, University of Reading, Reading, United Kingdom

(Manuscript received 15 July 2005, in final form 22 December 2005)

ABSTRACT

This article describes a novel algorithmic development extending the contour advective semi-Lagrangian model to include nonconservative effects. The Lagrangian contour representation of finescale tracer fields, such as potential vorticity, allows for conservative, nondiffusive treatment of sharp gradients allowing very high numerical Reynolds numbers. It has been widely employed in accurate geostrophic turbulence and tracer advection simulations. In the present, diabatic version of the model the constraint of conservative dynamics is overcome by including a parallel Eulerian field that absorbs the nonconservative (diabatic) tendencies. The diabatic buildup in this Eulerian field is limited through regular, controlled transfers of this field to the contour representation. This transfer is done with a fast newly developed contouring algorithm. This model has been implemented for several idealized geometries. In this paper a single-layer doubly periodic geometry is used to demonstrate the validity of the model. The present model converges faster than the analogous semi-Lagrangian models at increased resolutions. At the same nominal spatial resolution the new model is 40 times faster than the analogous semi-Lagrangian model. Results of an orographically forced idealized storm track show nontrivial dependency of storm-track statistics on resolution and on the numerical model employed. If this result is more generally applicable, this may have important consequences for future high-resolution climate modeling.

1. Introduction

This article describes a novel algorithmic development that opens up the possibility of using a highly efficient Lagrangian representation of finescale tracer fields, such as potential vorticity, in fully realistic numerical models of the atmosphere and oceans. This model, based on the contour advective semi-Lagrangian (CASL) model (Dritschel and Ambaum 1997, hereafter DA97), allows one to accurately simulate finescale flow structures (e.g., fronts) at modest grid resolutions. The model makes use of conventional numerical models for efficiency in computing the velocity field from the prognostic variables employed. It departs from conventional models in its representation of potential vorticity (and optionally other quasi-

conserved tracer fields) with a grid-free Lagrangian contour representation.

The original, conservative CASL model exploited the material conservation of potential vorticity (PV) by employing a contour representation of this field. Such a representation allows for unbounded, nondiffusive PV gradients (by collapsing together contours) without increased numerical cost. Furthermore, it allows for a purely advective time step, limited only by considerations of accuracy or by a condition on the Lifschitz number—generally a much weaker constraint than that imposed by a Courant–Friedrichs–Lewy (CFL) number (Smolarkiewicz and Pudykiewicz 1992; Dritschel and Ambaum 1998). Advantages of the CASL model over more conventional models are quantified in DA97, Dritschel et al. (1999), and Dritschel and Viúdez (2003). For multilayer high-resolution simulations of geostrophic turbulence the CASL model is orders of magnitude more efficient than the corresponding pseudospectral model.

The disadvantage of the original CASL model is its

Corresponding author address: Prof. David G. Dritschel, Mathematical Institute, University of St Andrews, St Andrews KY16 9SS, United Kingdom.
E-mail: dgd@mcs.st-and.ac.uk

inability to incorporate nonconservative effects. The fundamental problem is that the Lagrangian nature of CASL depends on the ability to evolve tracer fields by advecting its isolines. This property is lost because general nonconservative effects can produce nonadvective changes to the position of the isolines (e.g., the formation of new maxima or minima). A solution to this problem was presented in Dritschel and Ambaum (1998): their model ensures that as much as possible of the diabatic contribution to the PV field is represented by additional advective changes in the location of contours/isolines as well as by changes in the values of the PV that isolines represent. The residual contribution is then transferred to a secondary PV field q_d , the so-called diabatic PV, which is represented and evolved on an Eulerian grid using a conventional semi-Lagrangian model. The diabatic PV field is transferred back to the contoured field at later times where possible through additional advective and contour-level changes. The diabatic PV field suffers from the usual problems encountered by Eulerian models, in particular excessive numerical diffusion at moderate resolution. In the case presented in Dritschel and Ambaum (1998) this field was shown to remain small in amplitude and mainly broad in scale throughout the simulation, thus limiting the damage the Eulerian part did to the overall accuracy. However, the model remains unsatisfactory in that there is no control on the transfer between the Lagrangian and Eulerian PV fields, and, most seriously, not all of the nonadvective changes in PV can be accounted for by contour-level changes and additional advection.

Here, we describe a new extension to CASL that permits general, nonconservative processes to act on PV (such as thermal forcing and Ekman pumping). The extension preserves the ability of the model to represent PV well below grid scale, while fully accounting for nonconservative PV generation and destruction on each isentropic surface. In the next section we outline the implementation of this new model in a general quasigeostrophic context. In section 3 we present two cases of single-layer simulations of unstable barotropic jets, exploring the differences between the new model and pseudospectral and semi-Lagrangian models. Some concluding remarks are presented in section 4. The new model is much less affected by numerical diffusion than traditional Eulerian models. This is shown to have a substantial and highly nontrivial effect on the climate of the different model simulations.

2. Outline of the model

The quasigeostrophic model for the adiabatic case, the CASL model, is described in DA97. Here we focus

on the new elements needed to deal with diabatic forcing. For the moment, we leave the specific form of this forcing, denoted S below, arbitrary. However, we will implicitly assume that S is broad in scale so that it can be accurately represented on the underlying Eulerian grid. The next section considers a form commonly used in idealized studies.

Under the quasigeostrophic approximation, the prognostic equation for PV reads

$$\frac{Dq}{Dt} = q_t + uq_x + vq_y = S, \quad (1)$$

where $q = q(\mathbf{x}, t)$, and $S = S(\mathbf{x}, t)$ can depend on q (here and below the subscripts x , y , z , and t denote partial derivatives). From q , one may obtain the streamfunction $\psi(\mathbf{x}, t)$ by inverting the appropriate quasigeostrophic linear operator \mathcal{L} in the relation

$$\mathcal{L}\psi = q, \quad (2)$$

together with boundary conditions (as detailed for instance in the above reference). From ψ , one obtains the layerwise-two-dimensional incompressible flow field via

$$\mathbf{u}(\mathbf{x}, t) = (u, v) = (-\psi_y, \psi_x). \quad (3)$$

Equations (1)–(3) suffice to describe the flow evolution.

The original CASL model solves the above set for $S \equiv 0$. In the CASL model the contour representation of the PV field is converted to an appropriate grid representation by a novel contour-to-grid conversion algorithm. The streamfunction and velocity fields are then obtained by a fast inversion of this gridded PV field. The gridded velocity field is then interpolated to the contour node positions to find the velocities to advect the contours with. The grid representation of the PV field is a coarse-grained version of the contoured PV field, which conserves the required integral constraints. This coarse graining is allowed because the spectrum of \mathbf{u} is steeper than that of q . Details can be found in DA97.

The contour representation of the PV field contains a *surgical scale*, which may be thought of as the effective resolution of the model. Below the surgical scale, PV filaments are removed in a procedure called “surgery” (Dritschel 1989). Surgery paved the way for the practical use of contour dynamics models (Dritschel 1997). The current implementation of the surgery procedure is described in DA97. For a given numerical cost the surgical scale is much smaller than the grid scale in any Eulerian model. Note that the surgical scale does not limit the gradients of the PV field; these can become effectively infinite by collapsing together contours.

As in Dritschel and Ambaum (1998) the new model splits q into two fields, q_a and q_d , respectively called the adiabatic and diabatic PV fields. The two fields satisfy

$$\frac{Dq_a}{Dt} = 0 \quad \text{and} \quad \frac{Dq_d}{Dt} = S, \quad (4)$$

which, given $q = q_a + q_d$, satisfy Eq. (1). Note that the advecting velocity \mathbf{u} depends on the sum of q_a and q_d .

As q_a satisfies a conservative equation, we represent this field as contours, as in the original CASL model. However, for q_d , we use a conventional model, optionally pseudospectral or semi-Lagrangian. The rationale is that a conventional model is perfectly capable of evolving a broad-scale field, so long as it remains that way. And, a conventional model permits the uptake of diabatic forcing in a simple way. We start a simulation with $q_d = 0$ and $q_a = q(\mathbf{x}, 0)$. For $S \neq 0$, q_d will begin to develop, and then the advection implicit in the D/Dt operator will normally induce a scale cascade to small scales in the form of sharp PV gradients and filaments. This is something that is efficiently and accurately handled by contour advection, but *not* by conventional models. Hence, there is a limit to how long one can integrate before the diffusion in those models becomes important, thereby introducing additional, unwanted diabatic processes into the model.

To prevent this from happening, or from becoming practically significant, we limit the time integration to periods over which q_d is accurately evolved by those models, that is, during which q_d has little finescale structure. At the end of each such period, q_a and q_d are combined on an ultrafine grid—here 8 times finer than the grid used to compute \mathbf{u} . The associated grid length is comparable to the scale of surgery used to limit the width of contour filaments (in q_a). Then, a novel fast-contouring algorithm (using hash tables and avoiding conditional statements) is used to reconstruct a new set of contours, with equal spacing Δq in PV, that will become the initial q_a for the subsequent period of evolution.

It is then natural to reinitialize $q_d = 0$; however, instead q_d is initialized with the residual error left over from contouring a continuous field of data with a finite number of contours. This error is obtained by taking the difference of q_a after contouring and q before contouring on the inversion grid. To do this, q_a after contouring is momentarily converted to gridded values as in the original CASL model. This procedure ensures that the gridded PV at the end of one period is *identical* to that at the start of the next period. This is important in applications to more complete models, to prevent spurious generation of inertia-gravity waves.

The contouring procedure, while fast compared with other commonly available routines, is still costly when applied to a fine-resolution field of data, and therefore it should be done only when necessary. Furthermore, this procedure, if applied too often, prevents the natural tendency for q_a contours to collapse together (i.e., to form very steep PV gradients). In this respect, contouring appears to be slightly diffusive. Yet, the main object of this new model is to make numerical diffusion of any form much weaker than what takes place in conventional models. So contouring frequently can be diffusive for q_a , while contouring infrequently can be diffusive for q_d . Hence, one must choose an optimal period between contouring, Δt_{cont} , which minimizes the overall diffusion.

At present, in experiments with large-scale thermal forcing (see next section), by trial and error we have determined that Δt_{cont} should be proportional to the advective time scale t_{adv} , roughly the time it takes for a significant small-scale cascade to take place. The latter is chosen initially, from presumed knowledge of the basic flow characteristics—for example, $t_{\text{adv}} = 4\pi/Q$, where Q is the maximum PV amplitude at $t = 0$, or an expected maximum amplitude during the time evolution (Q , like q , has units of inverse time as is usual in the quasigeostrophic context).

Another important parameter (only when diabatic forcing is present and creating nonadvective changes to the PV) is the contour interval Δq . Small Δq means high resolution of the PV field, in a Lagrangian sense, just like a small grid length Δx means high resolution in an Eulerian sense. Very small Δq would give very high accuracy by allowing small variations of PV (e.g., created by the diabatic forcing) to be well resolved, but this would also be very costly. On the other hand, large Δq would be inaccurate but cheap. Hence, the choice of Δq is a compromise between accuracy and efficiency, and tests so far suggest that a sensible balance is achieved through the relation $\Delta q/Q \sim \Delta x/L$, where L is a horizontal length scale characterizing the PV distribution. This matches the Lagrangian resolution with the Eulerian resolution.

There are no other new parameters to consider for the implementation of diabatic forcing. As in the original CASL model, the time step Δt is chosen to be a small fraction of t_{adv} , and here we take $\Delta t \lesssim t_{\text{adv}}/40$ [in a third-order Adams–Bashforth time integration scheme, previously used in the shallow-water CASL model described in Dritschel et al. (1999)]. Surgery is performed at intervals of $\Delta t_{\text{surg}} = t_{\text{adv}}/8$, *except* when q_a and q_b are combined and contoured (which can be viewed as a kind of surgery). In fact, it is convenient to choose Δt_{cont} to be a multiple of Δt_{surg} , so that the con-

touring does the work of surgery every few times, typically every 8 times.

3. Numerical tests

a. Barotropically unstable jet

A number of tests have now been carried out, and here we present just two typical examples. We consider for simplicity a single-layer equivalent barotropic flow on the f plane, for which Eq. (2) becomes

$$\psi_{xx} + \psi_{yy} - \psi/L_R^2 = q, \quad (5)$$

where L_R is the radius of deformation. For the diabatic forcing S , we consider the commonly used idealized form for thermal damping,

$$S(\mathbf{x}, t) = \frac{\Psi(\mathbf{x}) - \psi(\mathbf{x}, t)}{\tau L_R^2}, \quad (6)$$

where τ is the radiative relaxation time scale and Ψ is a prescribed thermal equilibrium profile of the streamfunction (see, e.g., Ambaum 1997).

The domain is doubly periodic with x and y coordinates varying between $-\pi$ and π . The initial PV distribution is the same as used in Dritschel et al. (1999), but here in the quasigeostrophic context. It consists of a zigzag profile $q = q_0(y)$ between $y = -1$ and $y = 1$, with peak amplitude $Q = \pi/2$, and it induces a parabolic-like jet $u = u_0(y)$ flowing from left to right. This profile is disturbed initially by displacing each PV contour in y by the amount $(\sin 3x - \sin 2x)/20$. This is enough to trigger an instability with a reproducible initial structure.

Here, we choose $\Psi(\mathbf{x}) = \psi(\mathbf{x}, 0)$, so that the effect of the thermal damping is to relax the flow back to its initial (unstable) state. We take the radius of deformation $L_R = 0.5$, and the relaxation time $\tau = 20$ “days”.¹ Note that $t_{\text{adv}} = 8$ days and the time step $\Delta t = 0.2$ days.

We use a 64×64 doubly periodic domain in this and two other simulations conducted by the pure pseudospectral (PS) and pure semi-Lagrangian (SL) models. The new diabatic CASL model here uses the same semi-Lagrangian model for q_d [details may be found in Dritschel et al. (1999)]. In the PS simulation, $\nabla^6 q$ hyperdiffusion was added for numerical stability, and the time step was 10 times smaller than that used by the other two models, again for stability. Hyperdiffusion is convenient, though not consistent, as it results in sig-

nificant unphysical overshoots of advected fields (Yao et al. 1995; Dritschel et al. 1999). It is employed here simply because it is common practice.

The flow evolution shown in Fig. 1 illustrates the strong numerical diffusion present in the PS and SL models at this resolution [for further remarks, see Dritschel et al. (1999)]. While they produce similar results, they differ markedly from the CASL results. There are two main differences: first and most strikingly, the CASL results exhibit much more detailed structure (notice the “storms” along the flanks of the jet at 200 and 400 days); second, the CASL results exhibit much tighter PV gradients. Third, the overall structure of the PV field at later stages differs markedly from that in the other models. Of course, the nominal resolution of the three models is quite different: the surgical scale is a factor of 8 smaller than the grid scale. The smooth flow evolution seen in both the PS and SL results is the product of numerical diffusion, which is significant here. Both models strongly limit PV gradients and small-scale structure, albeit in different ways (hyperdiffusion for PS and interpolation-smoothing in SL).

Remarkably, for the chosen parameter settings, the net effect on the flow evolution is closely similar. However, this does not mean that either model is accurate—the results are highly sensitive to resolution, unlike in CASL (see Dritschel et al. 1999; Dritschel and Viúdez 2003; and below). In the next sections we present a more systematic exploration of model and resolution influence on the “climate” of the simulated fields.

The flow evolution to much later times (2500 days) shows vacillations (of about 300-days duration) between a nearly zonal state with a strong jet near $y = 0$ (stronger than that at $t = 0$ and with tighter PV gradients, at least in the CASL simulation), breaking down into a street of vortices having intense PV gradients at their edges, then collapsing back to the nearly zonal state. It would be interesting to explore how the time scale for this vacillation, and the amplitude of the excursions from the zonal state, depend on the basic parameters of the system, in particular L_R and τ .

b. Barotropic jet forced by orography

Here we present a more systematic exploration of the impact of the finescales resolved by the diabatic CASL model on the climate of the model. This is the first time we are able to do this in the context of a contour dynamics model because an adiabatic model simulating an unstable flow will develop decaying turbulence, which does not have a stable climate. A stable climate results from the equilibrium between turbulence and diabatic forcing. So the effect of resolution on the climate of a model is highly nontrivial.

¹ The nondimensional planetary vorticity f_0 is taken to be 4π , which makes the unit of time equal to a “day” in polar regions. Then, $Q = \pi/2$ corresponds to a Rossby number of 0.125.

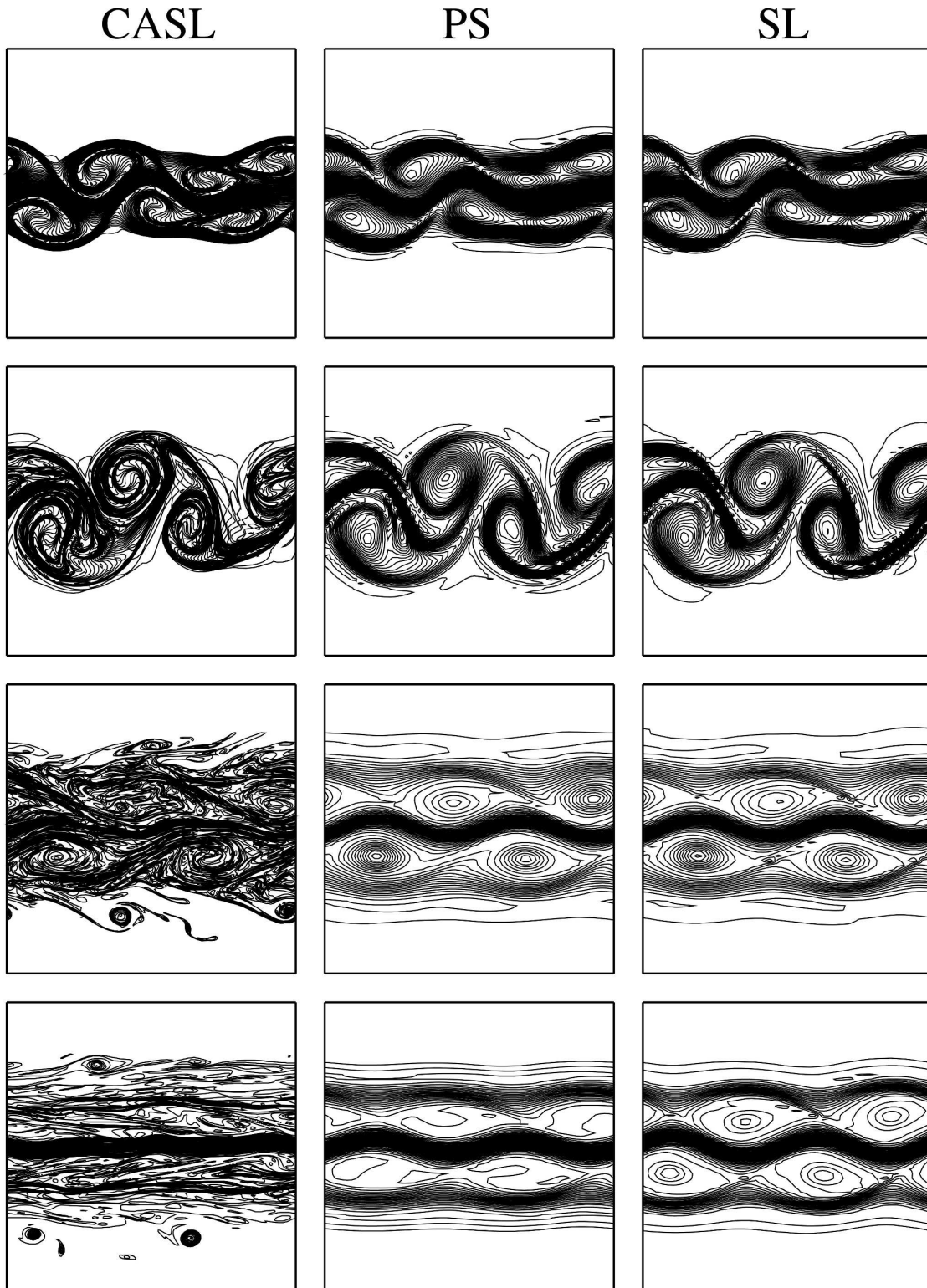


FIG. 1. (top to bottom) The PV field at 20, 40, 200, and 400 days for the (left to right) CASL, PS, and SL models.

As in section 3a, the initial flow is a zigzag profile in PV, but now without a wavelike lateral perturbation. Here, instead, the instability is induced by an elliptic Gaussian profile mountain of height η (nondimensionalized with the depth of the domain D) in the middle of the domain with half axes of length 0.2 in the x direction and 0.8 in the y direction and maximum height η_0 . The orography acts on the flow through a vortex stretching contributions to the PV:

$$q = \psi_{xx} + \psi_{yy} - \psi/L_R^2 + f_0\eta, \quad (7)$$

where $f_0 = 4\pi$ is the Coriolis parameter. The forcing is as in Eq. (6) with Ψ corresponding to the initial zonal jet PV profile in the absence of orography:

$$\Psi_{xx} + \Psi_{yy} - \Psi/L_R^2 = q(\mathbf{x}, 0). \quad (8)$$

We ran the diabatic CASL model with an underlying grid resolution of 128^2 and a surgical scale one-tenth of that. In parallel we ran the analogous semi-Lagrangian model at the same grid resolution and time step. Both models were run for 2500 days and the climate was defined as the average over the final 2000 days (climate is denoted by an overbar and anomalies from climate by a prime). The diagnostics are performed on the 128^2 grid for both models. We performed a suite of runs for varying relaxation time scale τ ($\tau = 3, 6, 12, 24$, and 48 days) and height of the orography η_0 ($\eta_0 = 1 \times 10^{-6}, 0.01, 0.02, 0.04, 0.08, 0.16$), a total of 30 runs.

Figure 2 shows the climate of the runs for a relaxation time scale of 3 days and a rescaled mountain height of 0.16. This is a strongly forced case for which it is not at all obvious that increased resolution is relevant. However, from the diagnostics in Fig. 2 it is clear that the effective change of resolution (a nominal factor of 10 between the CASL and SL models) has a strong impact on climate. The average PV \bar{q} has markedly sharper gradients and the eddy potential enstrophy q'^2 shows an increase downstream of the hill. The domain integrated eddy kinetic energy $\overline{u'^2 + v'^2}$ is close to a factor 3 times lower in the SL run compared with the CASL run. The zonal wind \bar{u} in the CASL run is stronger than that of the SL run and is supported by associated increased eddy momentum flux $\overline{u'v'}$ convergence.

Another strongly forced case, now for a relaxation time scale of 6 days and a rescaled mountain height of 0.04, is shown in Fig. 3. The differences in climate show a surprisingly different behavior to the previous case. The PV climate in the CASL run shows stronger gradients and generally a higher eddy potential enstrophy. However, both the eddy potential enstrophy and the eddy kinetic energy are markedly weaker right over the orography. As a result, the spatial average eddy kinetic

energy is about 10% higher in the SL run. This increased eddy kinetic energy is not associated with a stronger eddy momentum flux convergence: the zonal wind in the CASL run is stronger than in the SL run supported by the zonal eddy momentum fluxes.

Figure 4 presents an overview of the spatially averaged eddy kinetic energy variation over the suite of runs performed. It can be seen from the white contours in Fig. 4 that a strong thermal forcing generally leads to a weaker eddy kinetic energy. In this regime the thermal forcing dominates the inertial effects. The total eddy kinetic energy increases with longer relaxation scales and appears to peak around time scales of about 24 days. For even longer relaxation time scales the total eddy kinetic energy decreases again, presumably because of weaker winds as a result of weaker forcing.

The ratio of domain-integrated eddy kinetic energy between the SL and CASL runs is plotted as the shading in Fig. 4. This ratio shows a remarkably complex structure as a function of the parameters. The domain-integrated eddy kinetic energy is generally larger in the CASL runs than in the SL runs, up to a factor of 3 for the strongly forced, high-orography case. However in some parts of parameter space the SL runs show higher total eddy kinetic energy (higher by about 10%) specifically in the weak-forcing, low-orography cases. A local maximum of this ratio occurs at a relaxation time scale of 6 days and rescaled mountain height of 0.04.

c. Further resolution and convergence results

The climates of the CASL and SL runs are significantly different for all chosen parameters. This difference may be due to the lack of cross-gradient diffusion in the CASL model and the higher effective resolution. The difference in the climates appears to be a highly nontrivial function of the physical parameters of the system. One of the problems with these kinds of model comparisons is that the "truth" is not known. The best we can do is to look at convergence as well as compare the models with nominally similar resolutions.

In Fig. 5 we plot the difference between climates at two different model resolutions for the diabatic CASL and SL models. Both models were run on a 256^2 and a 128^2 grid and the diagnostics were produced on the 128^2 grid. As can be seen, the CASL model shows the smallest difference between the two resolutions indicating a higher convergence rate (consistent with earlier studies of unforced flows). We only show the PV climate in Fig. 5 but the other statistics lead to the same conclusion.

In Fig. 6 we compare the CASL and SL models at nominally similar resolution. The CASL model was run on a 64^2 grid and a surgical scale 8 times as small as the grid size. As the surgical scale is the nominal resolution

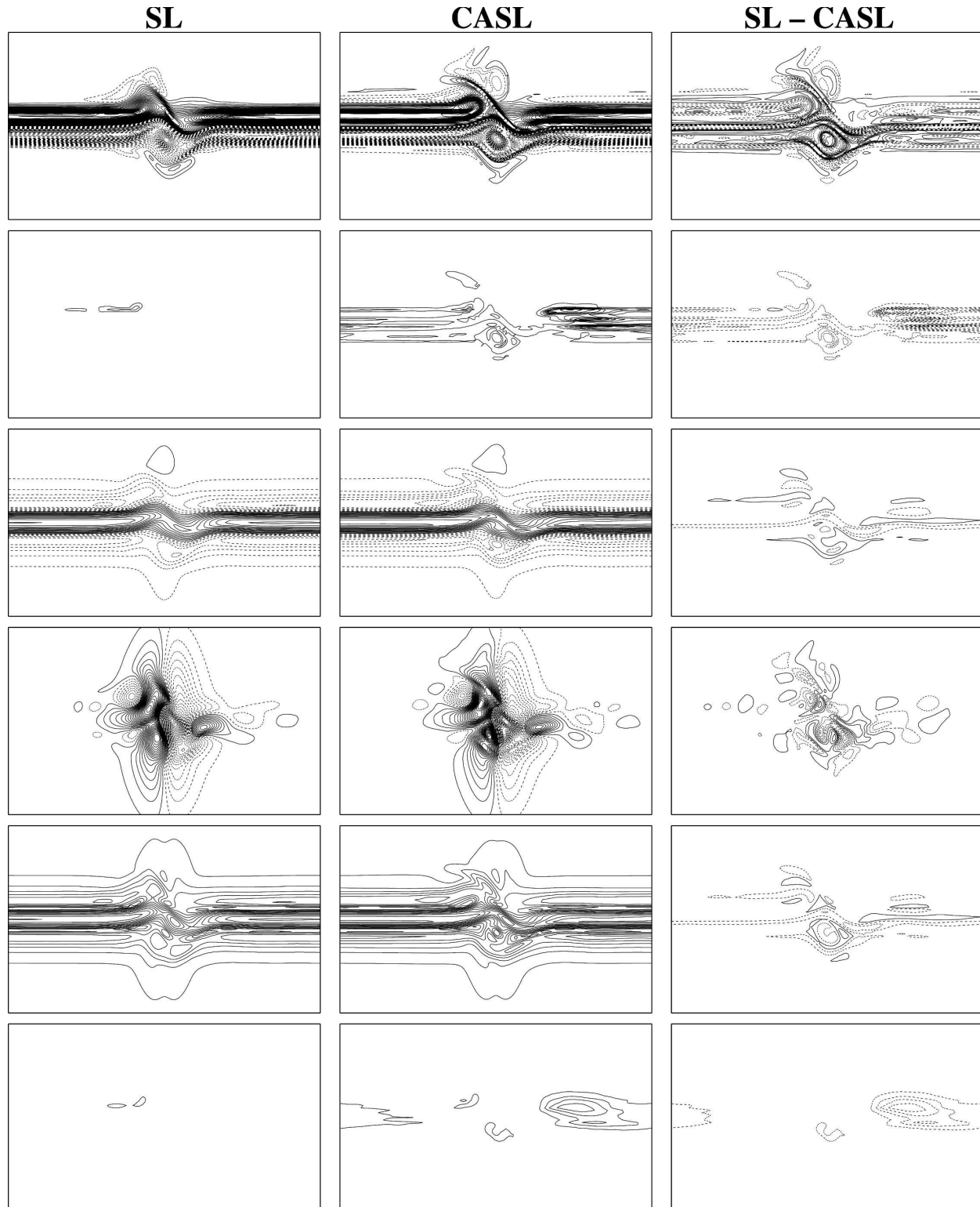


FIG. 2. Plots of (top to bottom) \bar{q} , $\overline{q'^2}$, \bar{u} , \bar{v} , $\overline{u'v'}$, and $\overline{u'^2 + v'^2}$ for the (left to right) SL and CASL models and SL-CASL for $\tau = 3$ days and $\eta_0 = 0.16$. Contour intervals are (top to bottom) 0.05, 0.01, 0.01, 0.0025, 0.01, and 0.000025.

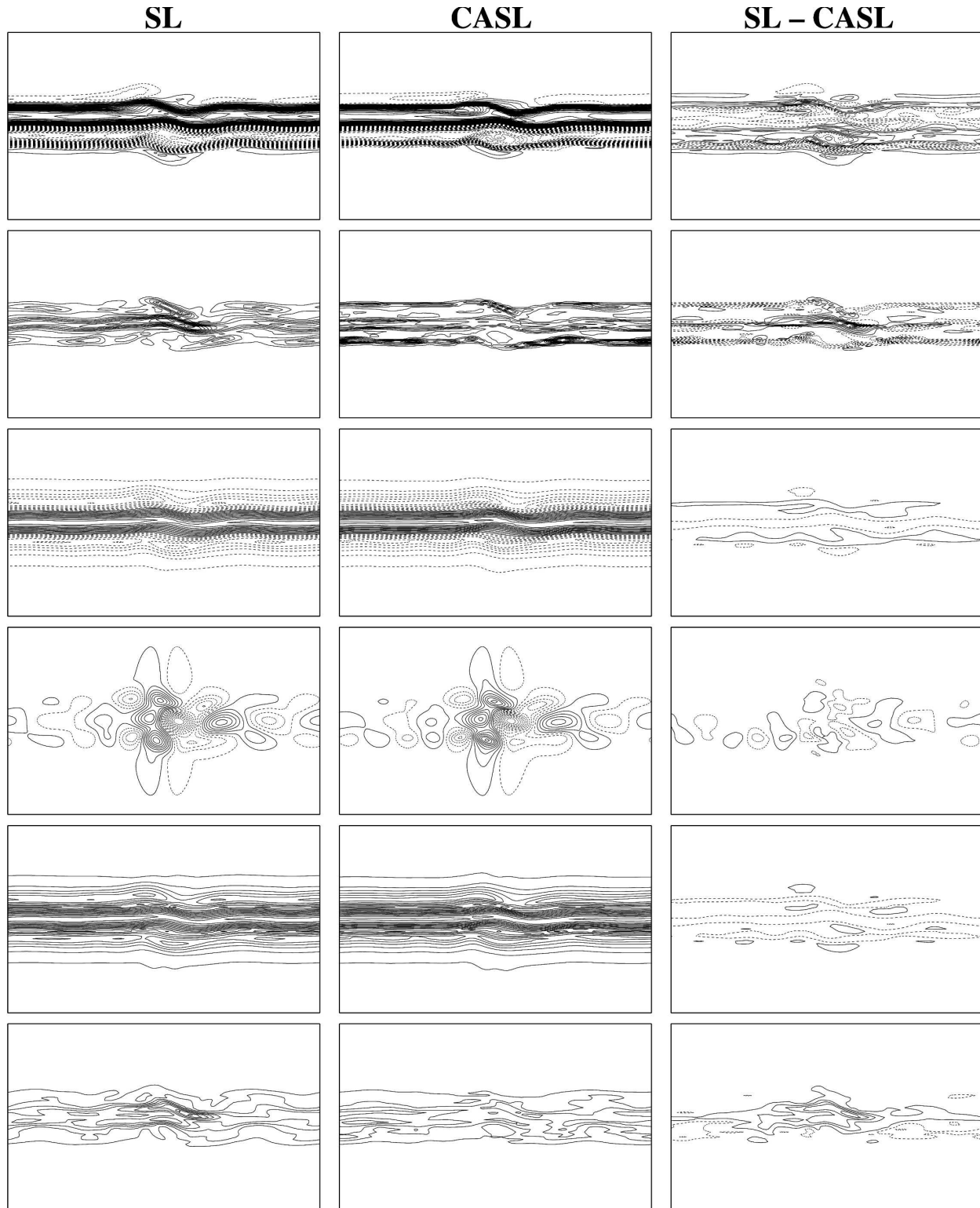


FIG. 3. Plots of (top to bottom) \bar{q} , $\overline{q'^2}$, \bar{u} , \bar{v} , $\overline{u'v'}$, and $\overline{u'^2 + v'^2}$ for the (left to right) SL and CASL models and SL-CASL for $\tau = 6$ days and $\eta_0 = 0.04$. Contour intervals are the same as in Fig. 2.

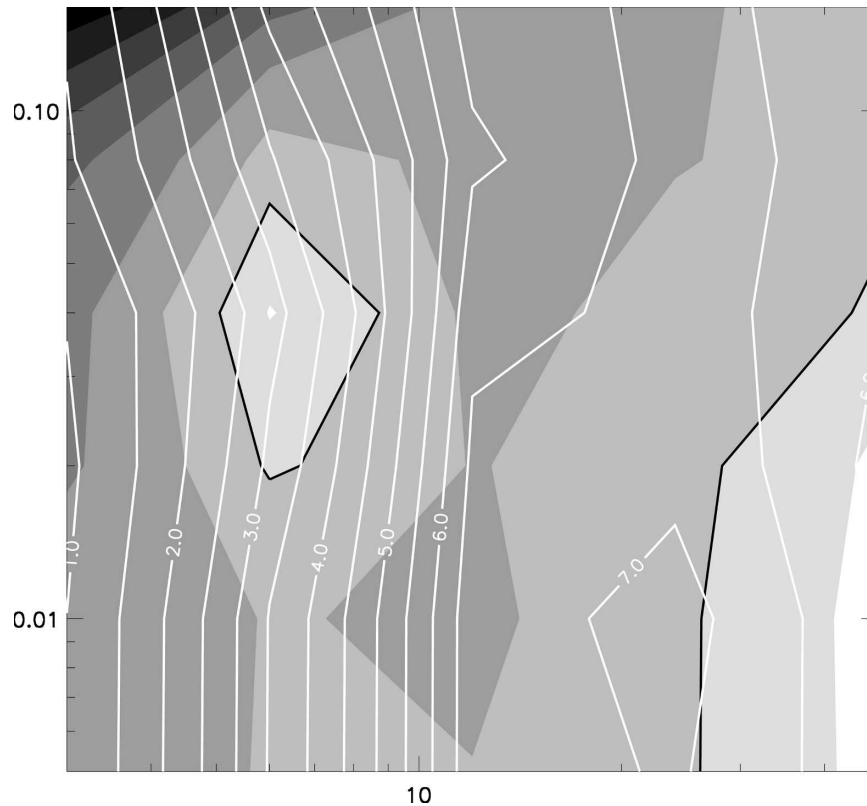


FIG. 4. Eddy kinetic energy diagnostics for all runs. Here the x axis is relaxation time scale τ in days, and the y axis is nondimensional mountain height η_0 . The relative magnitude of spatially averaged eddy kinetic energy of the CASL and SL runs is shown with shading. The darker shading corresponds to lower magnitudes in the SL run (minimum of 0.32), lighter shading to higher magnitudes (maximum of 1.14). The black contour corresponds to equal magnitudes. White contours indicate spatially averaged eddy kinetic energy in the CASL runs.

of the CASL model (even though infinitely large gradients are possible by collapsing contours) we compare this with a semi-Lagrangian run at 512^2 grid resolution. The CASL run took about 1500 s on a single processor machine with 1.3-GHz clock speed while the SL run took 40 times as long to run on the same machine. It is clear from Fig. 6 that the two climates are not the same even though their nominal resolutions are similar. This is a puzzling finding with obvious implications for climate modeling.

4. Summary and discussion

We have introduced a new extension of the CASL model that incorporates diabatic forcing while retaining the advantages of the original model, namely, the ability to efficiently and accurately capture abundant fine-scale PV and sharp PV gradients. The new extension retains the efficiency and conservative nature of a contour representation of the PV field. Nonconservative

effects are accumulated in a so-called “diabatic” PV field, which is evolved by a traditional Eulerian model, here a semi-Lagrangian one. To prevent unwanted numerical dissipation, the diabatic PV field is periodically transferred to the contoured PV field through a highly efficient new contouring algorithm especially developed for this application.

We have presented two demanding test cases comparing our new model with more traditional models.² In the first case of a forced unstable barotropic jet, we found that the PV field in the CASL model is broadly similar to that in the semi-Lagrangian and pseudospectral models initially, but in time smaller-scale differences accumulate to produce a substantially different flow structure characterized by much tighter PV gradi-

² One of the reviewers pointed out potential similarities with hybrid-level set methods (Enright et al. 2002). Because these methods have not yet been used in geophysical flows of interest a comparison with such methods could not be performed.

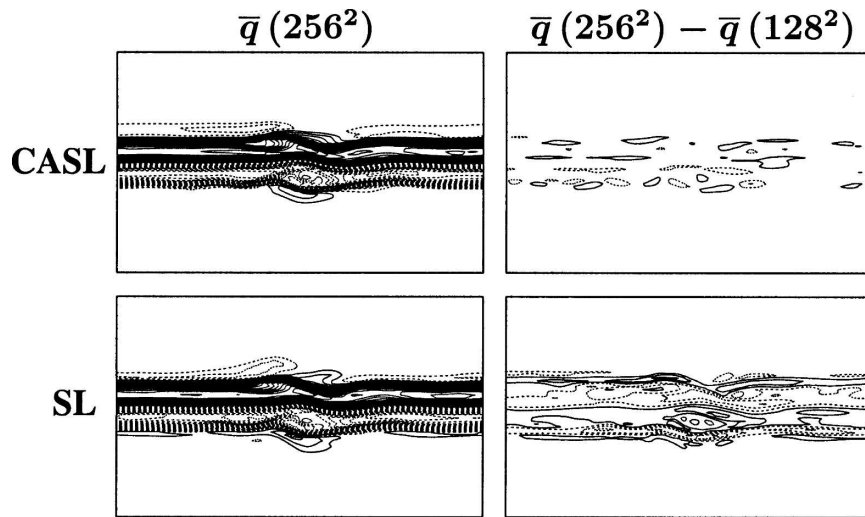


FIG. 5. The PV climate at 256^2 grid resolution in (top left) CASL and (bottom left) SL, and differences from the PV climate at 128^2 grid resolution in (top right) CASL and (bottom right) SL for $\tau = 6$ days and $\eta_0 = 0.04$. The diagnostics were produced on the 128^2 grid. The contour interval is 0.05 in all panels.

ents in the CASL model and a wealth of small-scale variability virtually absent in the Eulerian models.

In the second test case, we examined a forced unstable barotropic jet perturbed by orography. We charted the “storm track” behavior of the CASL and analogous semi-Lagrangian models for different relaxation time scales and mountain heights. The differences in climate between the two models are marked, especially in eddy diagnostics. Overall, the CASL model shows higher eddy activity than the semi-Lagrangian model, most notably in strongly forced cases. There are, however, areas in parameter space where the semi-Lagrangian model exhibits larger eddy activity as measured by the area-averaged eddy kinetic energy. In all instances the spatial structure of the eddy field (storm track) is significantly different between the models.

We also compared the convergence of the models with increasing resolution and the convergence between the models at the same nominal resolution for the unstable barotropic jet perturbed by orography. The CASL model was found to converge markedly faster than the semi-Lagrangian model with increasing resolution. Furthermore, at the same nominal resolution the CASL model ran 40 times faster than the semi-Lagrangian model. Additionally, at the same nominal resolutions the two models showed differing climates.

The change from a semi-Lagrangian model to a non-diffusive, high-resolution CASL model gives substantial and a priori unpredictable changes in the simulated storm track. This should serve as a cautionary tale for the use of current climate models to look at storm-track

behavior and extreme weather in changed climates. The dynamical cores of these climate models are essentially similar to the semi-Lagrangian model we used here to compare with our extended CASL model. Even “simple” changes to current climate models, such as resolution, may have unpredictable effects on the storm-track climate.

We have restricted our forcing field S to large spatial scales. This ensures that the mixdown time of the diabatic PV field is substantial compared with a time step so that the number of recontouring steps can be limited. This may be viewed as a limitation of the CASL model. However, the large spatial scale for S is not a requirement for the CASL model to work. Furthermore, the mixdown problem is even worse in Eulerian models of similar resolution because no mechanism exists to transfer diabatic PV to a nondiffusive Lagrangian representation. Those models would simply diffuse more, adding an unwanted diabatic source.

The setup of our extended CASL model can be employed trivially to evolve tracer fields other than PV. Hence this model can serve as a tracer transport model in atmospheric chemistry models. The effectiveness of a contour representation for passive tracers has been convincingly demonstrated by several papers starting from work by Waugh and Plumb (1994) and Norton (1994). The forcing field S represents the chemical transitions of the advected species. Both the advective field and the forcing field could be prescribed such that the extended CASL model runs offline.

We have presented here the single-layer doubly pe-

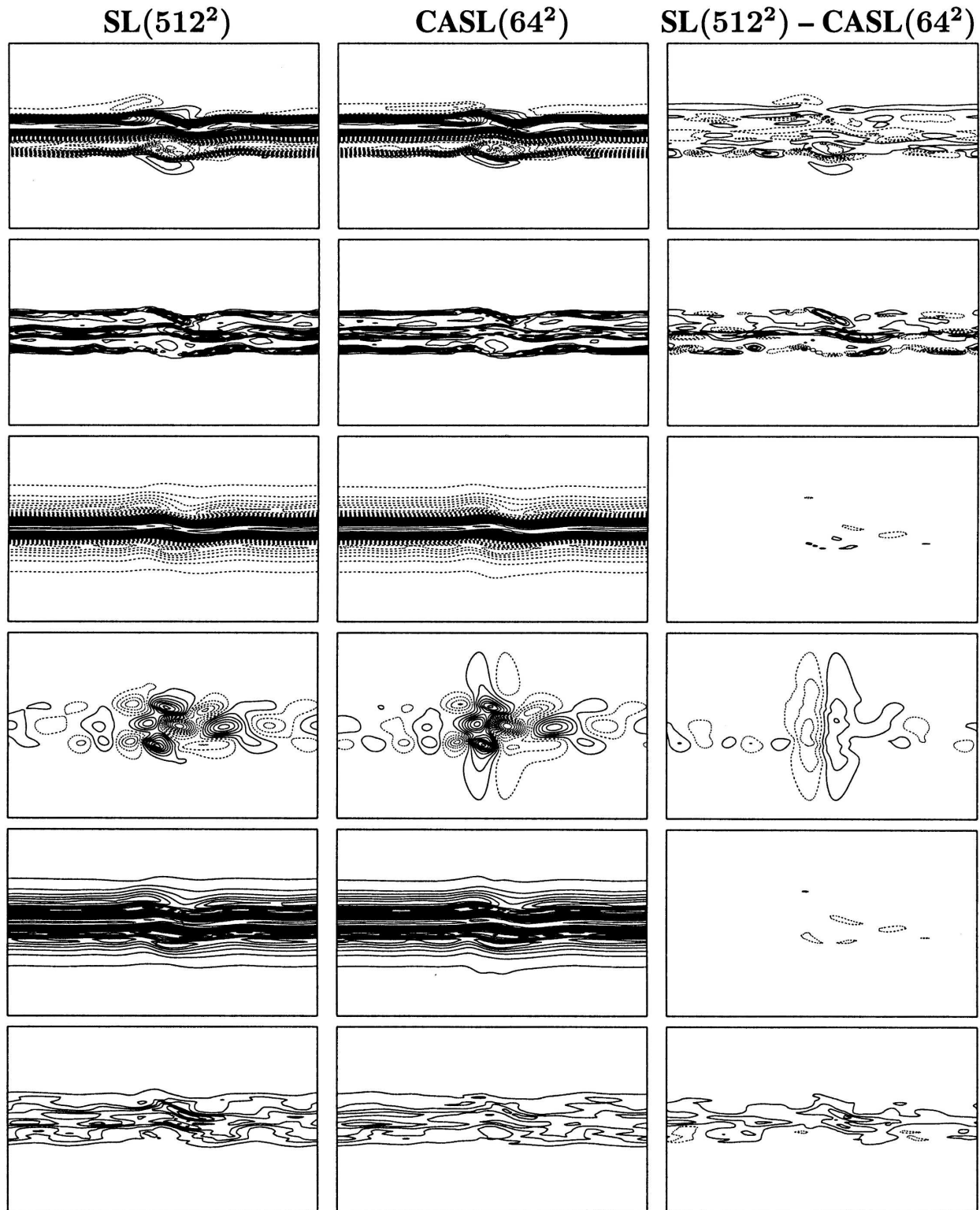


FIG. 6. Plots of (top to bottom) \bar{q} , $\overline{q'^2}$, \bar{u} , \bar{v} , $\overline{u'v'}$, and $\overline{u'^2 + v'^2}$ for (left to right) SL at 512² grid resolution, CASL at 64² grid resolution, and SL-CASL for $\tau = 6$ days and $\eta_0 = 0.04$. The diagnostics for both models are calculated on the 64² grid. The contour intervals are the same as in Fig. 2.

riodic implementation of the extended CASL model to provide a proof of concept in the simplest possible implementation. However, currently a multilayer model exists and a spherical shallow-water model is being developed. An exciting interpretation of the forcing field in the multilayer model is the transfer of “PV substance” (Haynes and McIntyre 1987) between different isentropic layers. Modifications of our model to different horizontal geometries are technical exercises. Extensions to more “realistic” models (e.g., primitive equation, nonhydrostatic) can be followed through as in Dritschel et al. (1999). This would open the way to using the CASL model as a dynamical core of a general circulation model.

REFERENCES

- Ambaum, M. H. P., 1997: Isentropic formation of the tropopause. *J. Atmos. Sci.*, **54**, 555–568.
- Dritschel, D. G., 1989: Contour dynamics and contour surgery: Numerical algorithms for extended, high-resolution modeling of vortex dynamics in two-dimensional, inviscid, incompressible flows. *Comput. Phys. Rep.*, **10**, 77–146.
- , 1997: Introduction to “Contour dynamics for the Euler equations in two dimensions.” *J. Comput. Phys.*, **135**, 217–219.
- , and M. H. P. Ambaum, 1997: A contour-advective semi-Lagrangian algorithm for the simulation of fine-scale conservative fields. *Quart. J. Roy. Meteor. Soc.*, **123**, 1097–1130.
- , and —, 1998: The inclusion of non-conservative forcing into a conservative contour advection algorithm. *Numerical Methods for Fluid Dynamics IV*, M. J. Baines, Ed., ICFD, 99–110.
- , and A. Viúdez, 2003: A balanced approach to modelling rotating stably-stratified geophysical flows. *J. Fluid Mech.*, **488**, 123–150.
- , L. M. Polvani, and A. R. Mohebalhojeh, 1999: The contour-advective semi-Lagrangian algorithm for the shallow-water equations. *Mon. Wea. Rev.*, **127**, 1151–1165.
- Enright, D., R. Fedkiw, J. Ferziger, and I. Mitchell, 2002: A hybrid particle level set method for improved interface capturing. *J. Comput. Phys.*, **183**, 83–116.
- Haynes, P. H., and M. E. McIntyre, 1987: On the evolution of vorticity and potential vorticity in the presence of diabatic heating and friction or other forces. *J. Atmos. Sci.*, **44**, 828–841.
- Norton, W. A., 1994: Breaking Rossby waves in a model stratosphere diagnosed by a vortex-following coordinate system and a technique for advecting material contours. *J. Atmos. Sci.*, **51**, 654–676.
- Smolarkiewicz, P. K., and J. A. Pudykiewicz, 1992: A class of semi-Lagrangian approximations for fluids. *J. Atmos. Sci.*, **49**, 2082–2096.
- Waugh, D. W., and R. A. Plumb, 1994: Contour advection with surgery: A technique for investigating finescale structure in tracer transport. *J. Atmos. Sci.*, **51**, 530–540.
- Yao, H. B., D. G. Dritschel, and N. J. Zabusky, 1995: High-gradient phenomena in two-dimensional vortex interactions. *Phys. Fluids*, **7**, 539–548.